fibers

MDPI

Article

Cotton Cellulose-CdTe Quantum Dots Composite Films with Inhibition of Biofilm-Forming *S. aureus*

Rohan S. Dassanayake [1,2], Poorna T. Wansapura [1,2], Phat Tran [2], Abdul Hamood [3] and Noureddine Abidi [1,*]

1 Fiber and Biopolymer Research Institute, Texas Tech University, Lubbock, TX 79409, USA; rdassanayake@ithaca.edu (R.S.D.); tharakawansha@gmail.com (P.T.W.)
2 Department of Ophthalmology and Visual Sciences, Texas Tech University Health Sciences Center, Lubbock, TX 79430, USA; phat.tran@ttuhsc.edu
3 Department of Immunology and Molecular Microbiology, Texas Tech University Health Science Center, Lubbock, TX 79430, USA; abdul.Hamood@ttuhsc.edu
* Correspondence: noureddine.abidi@ttu.edu

Received: 15 May 2019; Accepted: 11 June 2019; Published: 19 June 2019

Abstract: A cellulose-cadmium (Cd)-tellurium (TE) quantum dots (QDs) composite film was successfully synthesized by incorporating CdTe QDs onto a cellulose matrix derived from waste cotton linters. Cellulose-CdTe QDs composite film was characterized by field emission scanning electron microscopy (FE-SEM), energy dispersive X-ray (EDX) spectroscopy, Fourier transform infrared (FTIR) spectroscopy, thermogravimetric analysis (TGA), and X-ray diffraction (XRD). The antibacterial activity of the prepared composite film was investigated using the multidrug-resistance (MTR) *Staphylococcus aureus* bacteria. In vitro antibacterial assays demonstrated that CdTe QDs composite film can efficiently inhibit biofilm formation. Our results showed that the cellulose-CdTe QDs composite film is a promising candidate for biomedical applications including wound dressing, medical instruments, burn treatments, implants, and other biotechnology fields.

Keywords: cellulose; dissolution; CdTe quantum dots; antimicrobial film

1. Introduction

The Gram-positive (+*ve*) bacteria *Staphylococcus aureus* (*S. aureus*) is one of the widespread human pathogens and approximately 30–60% of the human population is intermittently or permanently colonized with *S. aureus* [1,2]. It is a prominent cause of many clinical infections including bacteremia, infective endocarditis, pneumonia, cellulitis, skin and soft tissue, pleuropulmonary, osteoarticular, hospital and medical device-related infections [1–4]. *S. aureus* is also considered as a well-known antibiotic resistance bacteria due to its ability to develop adaptive countermeasures against multiple antibiotics [5,6]. Especially, methicillin-resistant *S. aureus* (MRSA) strains are the main cause of antibiotic-resistant nosocomial infections worldwide. Biofilm formation on abiotic and biotic surfaces is an imperative virulence factor for *S. aureus* [7]. Biofilms form protective layers for bacterial proliferations, leading to persistent infection. Biofilms are an assemblage of bacterial cells enclosed in a self-produced extracellular polymer matrix and are more resistant to the human immune system, antibiotics, and sanitation agents [8–10]. Therefore, the treatment of *S. aureus* infections is extremely challenging and it is an increasing concern to the health sector [9,11].

Cellulose is the most abundant natural polymer on earth. It is a polysaccharide consisting of many linear homopolymer of D-anhydroglucopyranse units linked by β (1→4) linked D-glucose units [12,13]. Cellulose can be extracted from plants such as wood, cotton, flax, hemp, jute or ramie, and bacteria. Cotton is an important worldwide cash crop and is considered as a ubiquitous natural resource offering

the purest form of cellulose in nature [12,13]. Cellulose fiber inherits intriguing properties including relative abundance, biocompatibility, low density and high strength, thermal and mechanical stability, nontoxicity, low cost, and good sorption properties. Therefore, it has been used in many industries such as textile, food, energy, and medicine [14–17].

Over the past few years, there have been many investigations of cellulose-based composite materials as antimicrobial agents against many antibiotic resistance pathogens including *S. aureus* [18–20]. However, cellulose and its derivatives do not intrinsically show antipathogenic properties. Therefore, the antimicrobial properties have been achieved either by chemical modification of cellulose with unique antimicrobial functional properties or incorporating antimicrobial agents. Cellulose functionalized with amino groups and aminoalkylsilane groups have been reported as antimicrobial agents against *S. aureus* [21–24]. Cellulose composites impregnated with nanoparticles including Ag [25,26], Cu [27,28], TiO_2 [29,30], and ZnO [31,32] have also been investigated as antimicrobial agents against *S. aureus*.

Quantum dots (QDs) have received a significant attention in the biomedical field as they possess distinct characteristics over other luminescent materials [33–35]. QDs have been widely used for preparing solar cells [36,37], photonic crystal devices including light-emitting diodes [38], and fluorescent probes in cell imaging [39,40]. QDs possess greater brightness, better photochemical stability, water solubility, robust fluorescent intensity, high quantum yields, a broad excitation wavelength range, tunable emission wavelengths, and size-tunable photoluminescence [35,41]. QDs are a class of semiconducting nanoparticles prepared from chalcogenides such as selenides, tellurides, and from sulfides of metals such as cadmium, zinc, lead, and copper [42,43]. The typical diameter of a quantum dot is in the range of 1–10 nanometers [43]. Recently, the antibacterial effect of QDs against gram-positive multi-drug resistance (MDR) bacteria such as *S. aureus* has also been reported [33,34,44]. However, there has been a great deal of concern over the use of QDs in living cells due to their poor biocompatibility, self-agglomeration, and instability in solution. Several approaches including coating QDs with biocompatible and biodegradable polymers and anchoring on a polymer matrix have been developed to overcome these issues.

In the current study, we investigate the effectiveness of glutathione (GSH)-capped CdTe QDs supported on cellulose films in inhibiting the development of multidrug resistance (MDR) *S. aureus* biofilms. Cellulose films were prepared from a facile method using waste cotton linters. To our knowledge, this is the first attempt to use waste cotton cellulose-CdTe QDs composite films as an anti-biofilm agent against *S. aureus*.

2. Experimental

Unless mentioned otherwise, all chemicals were purchased from Sigma-Aldrich (St. Louis, MO, USA). Waste cotton linters were received from the Fiber and Biopolymer Research Institute at Texas Tech University (Lubbock, TX, USA). LB and LB-Agar media were purchased from MP Biomedicals (Solon, OH, USA).

2.1. Synthesis of Glutathione (GSH) Capped-CdTe QDs

CdTe QDs were synthesized as described previously [45,46]. The general reaction involved the reduction of tellurium oxyanions by glutathione (GSH) in the presence of cadmium chloride at pH 9.0 citrate-borax buffer. In a typical experiment, stock solutions of 30 mM citrate-borate buffer (pH 9.0, 30 mM sodium borate $Na_2[B_4O_5(OH)_4]\cdot 8H_2O$, 30 mM sodium citrate ($Na_3C_6H_5O_7$ $2H_2O$), 7 mM potassium tellurite (K_2TeO_3), 30 mM reduced GSH, and 25 mM cadmium chloride ($CdCl_2$) were prepared. Then, 36.4 mL of 30 mM citrate-borate solution, 33.3 mL of 30 mM GSH, and 16.0 mL of 25 mM $CdCl_2$ were thoroughly mixed in a round bottom flask and the mixture was allowed to sit for 5 min at room temperature (RT). To this, 14.3 mL of 7 mM K_2TeO_3 were added to the mixture with continuous stirring. The molar ratio of $CdCl_2$:GSH:K_2TeO_3 was 4:10:1. To obtain QDs with desired emission color, the mixture was refluxed at 90 °C for 2 h to initiate QD nucleation. CdTe colloidal

solution was observed under long UV light at 365 nm. A sharp green fluorescence was observed. Synthesized CdTe QDs were separated with two volumes of ethanol and centrifuged for 30 min at 3500 rpm before being powdered and dried for 24 h in a desiccator over calcium chloride.

2.2. Scouring and Bleaching Process of Waste Cotton

Waste raw color cotton fibers were subjected to scouring and bleaching process to remove all non-cellulosic materials. First, 10 g of waste cotton fibers were soaked in a 1 L solution of non-ionic wetting agent (Triton X-100, 1 g/L) and NaOH (4 g/L). The mixture was heated at 90 °C for 1 h to facilitate the scouring process. Scoured cotton fibers were then rinsed with tap water for 10 min. These washed fibers were added to a 1 L solution of non-ionic wetting agent (Triton X-100, 0.25 g/L), NaOH (0.35 g/L), Na_2CO_3 (0.7 g/L), Na_2SiO_3 (3 g/L) and bleach (6 g/L) and heated at 90 °C for 1 h to conduct the bleaching process. The fibers were again thoroughly rinsed with hot tap water for 20 min to remove unreacted material. White color cotton fibers were then dipped and agitated in a 1 L glacial acidic acid solution (0.25 g/L) for 10 min to neutralize the pH. After that, the fibers were thoroughly washed with hot water and then distilled water for 20 min. Then, fibers were kept on a strainer to drain water. The wet fibers were kept in freezer at −20 °C for 2–4 h prior to freeze-drying. Then the fibers were subjected to a freeze-drying process at −105 °C for 48 h. Finally, the freeze-dried cotton fibers were powered using a Wiley mill with 40-mesh size (420 μm).

2.3. Preparation of Cellulose-GSH Capped CdTe QDs Composite Films

Cellulose-CdTe QDs composite films were prepared using a slightly modified method [44]. First, the crushed cellulose powder (5% *w*/*w*) was dispersed in a 100 mL of NaOH/Urea/H_2O solution (11:4:80% (*w*/*w*)) and stirred for 20 min. The mixture was then stored at −10 °C for 24 h. Then, the frozen mixture was thawed and stirred vigorously at RT for 2 h. After that, the mixture was again stored at −10 °C for 24 h. The frozen mixture was thawed and stirred vigorously at RT until the solution became transparent.

GSH capped CdTe QDs (1% *w*/*w* w.r.t cotton weight) was dispersed in the cellulose solution and stirred for 30 min. Then, epichlorohydrin (ECH) cross-linker (8 mL) was added dropwise to the mixture while stirring. The mixture (cellulose-CdTe QDs) was further stirred for 30 min and heated at 70 °C for 4 h. After that, the cellulose-CdTe QDs composite mixture was poured into Petri dishes and kept in an oven at 50 °C to 2 h to form a gel. Cellulose-CdTe QDs composite film was obtained by submerging the films in a distilled water bath and rinsing them with distilled water for 3 days. Finally, the composite films were air dried in an ambient air.

2.4. Material Characterization

2.4.1. Field Emission Scanning Electron Microscopy (FE-SEM) Imaging and Energy Dispersive X-ray (EDX) Analysis

The morphological analysis of the cellulose and cellulose-CdTe QDs composite films was conducted using a high-resolution Hitachi S-4700 FE-SEM. This instrument is also equipped with an EDX analyzer with a 30° take-off angle for collecting quantitative data, digital mapping, and X-ray images. Samples were sputter coated with gold and the edges were covered with copper tapes to achieve better SEM images.

2.4.2. Fourier Transform Infrared (FTIR) Spectroscopy

FTIR spectra were acquired using a PerkinElmer Spectrum-400 FTIR spectrometer (PerkinElmer, Waltham, MA) attached to a universal attenuated total reflectance accessory (UATR). This instrument is also equipped with a ZnSe-diamond crystal, which allow spectra acquisition from the sample without any preparation. All spectra were collected at a resolution of 4 cm^{-1} with 32 co-added scans

in the wavenumber range 4000–650 cm^{-1}. PerkinElmer Spectrum software was used to analyze the spectral data.

2.4.3. Thermogravimetric (TG) Analysis

High-resolution TG profiles of cellulose-CdTe QDs and cellulose films were studied using a PerkinElmer Pyris1TGA instrument furnished with a 20-sample auto-sampler. TG profiles were recorded in the temperature range of 37 to 600 °C in a nitrogen atmosphere (20 mL/min) at a heating rate of 10 °C/min. All data were analyzed using Pyris Data Analysis software. The TG profiles were recorded to investigate the thermal stability of the films.

2.4.4. X-ray Diffraction (XRD) Studies

X-ray diffraction (XRD) studies were conducted using a SmartLab XRD system (Rigaku Corporation, ModelHD2711N, The Woodlands, TX, USA). CuK_{α} (1.541867 Å) radiation was generated at a voltage of 40 kV and a tube current of 44 mA. Scanning was held continuously at a speed of 10°/min and the diffraction intensities were collected at a scan step of 0.010 between $2\theta = 10°$ and 50°.

The samples were conditioned at a relative humidity of 65 ± 2% and at a temperature of 21 ± 1 °C for 48 h prior to analysis.

2.4.5. Bacterial Strains, Media, and Growing Conditions

Gram-positive *S. aureus* GFP AH133 strain was grown in Luria Bertani (LB) broth or on LB agar plates at 37 °C with shaking (250 rpm). The strain carries plasmid pCM11 in which the gene that codes for green fluorescent protein (GFP) is constitutively expressed [44,47]. To maintain the plasmid pCM11 in *S. aureus* GFP AH133, 1 μg/mL erythromycin (AH133) was added to the LB broth.

2.4.6. Agar Diffusion Assay

The zone of inhibition of *S. aureus* by cellulose-CdTe QDs composite films was evaluated using an agar diffusion assay as described earlier [44,47]. First, the *S. aureus* strain was grown in LB broth supplemented with erythromycin at 37 °C overnight with shaking. The culture was then thoroughly washed with a pH 7.4 phosphate buffered saline (PBS) solution. Then, the inocula (approximately 10^8 colonies forming units (CFU)/mL) were prepared by diluting the *S. aureus* culture to an optical density at 600 nm (OD_{600}) of 0.5–0.6. An aliquot (100 μL) of the diluted culture was spread on the LB agar plate. After inoculation, three disks of cellulose-CdTe QDs composite films were placed on the plate. The diameter and thickness of each film were 6 and 1 mm, respectively. A parallel control experiment was also conducted with cellulose disks without QDs. The plates were then incubated at 37 °C for 24 h. Finally, the diameters of the zones of inhibition were measured to the nearest millimeter with a ruler.

2.4.7. Quantitative Analysis of the Biofilms (CFU/Disk)

The biofilm formation by *S. aureus* was quantified using the microtiter plate assay [44,47]. Biofilms were quantified by calculating the number of colony forming units per disk (CFU/Disk). Cellulose-CdTe QDs and cellulose disks were incubated in 1 mL of LB broth media in the presence of *S. aureus* (approximately 10^2–10^3 CFU) in the wells (1 disk per well) of 24-well microtiter plate. The microtiter plate was then incubated at 37 °C for 24 h under aerobic conditions. Then, each disk was removed from the well, rinsed with sterile distilled water, and placed in a 1.5 mL microcentrifuge tube containing 1 mL of PBS solution. The tubes were then sonicated for 10 min to loosen cells, followed by vortexing vigorously 3 times for 1 min to break up the biofilm and to detach the bacterial cells from the disk. Suspended cells were serially diluted 10-fold in PBS solution, and 10 μL aliquots of each dilution were spotted onto LB agar plates. These plates were then incubated at 37 °C for 24 h under aerobic conditions prior to the CFU counting. CFU per disk was calculated using the formula: CFU × dilution factor × 100. All experiments were conducted at least three times.

2.4.8. Analysis of the Biofilms by Confocal Laser Scanning Microscopy (CLSM)

The formation of biofilms was further investigated using a Nikon Eclipse Ni-E upright CLSM (Nikon Inc., Melville, NY, USA). The extent of the biofilm development by *S. aureus* GFP AH133 was observed under CLSM. The three-dimensional images of the biofilms were processed and analyzed using NIS-Elements 2.2 software.

2.4.9. Statistical Analysis

CFU assays were analyzed using the PrismVR version 4.03 (GraphPad Software, San Diego, CA, USA) with 95% confidence intervals. A comparison of the biofilms formed on the disks was performed using, unpaired two-tailed t-test.

3. Results and Discussion

3.1. Morphology Study

Figure 1 shows digital images of the prepared cellulose-CdTe QDs composite film and cellulose film under room light. The yellow color of the cellulose-CdTe QDs film is due to the presence of CdTe QDs. Under UV light irradiation at 365 nm wavelength, cellulose-CdTe QDs composite film exhibited an intense yellowish green fluorescence, see Figure 1a. This indicates that CdTe QDs form a photostable composite with cellulose polymer without deterioration of photoluminescence during the process of composite formation. However, cellulose without QDs did not fluoresce under UV light, see Figure 1b.

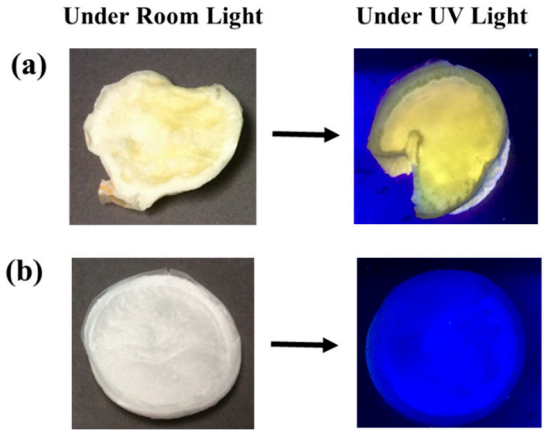

Figure 1. Digital photographs of the films under room light and UV light (**a**) cellulose-cadmium-tellurium quantum dots (cellulose-CdTeQD) and (**b**) cellulose film.

3.2. FESEM Images and Elemental Analysis

FESEM and EDX analysis were conducted to study the morphological features and elemental distribution of the samples. Figure 2 exhibits FESEM images of celluose-CdTe QDs composite film and cellulose film. As shown in Figure 2a, CdTe QDs are uniformly distributed within cellulose polymer matrix. The particle size of the QDs anchored is in 2–30 nm range. This is also an indication of the existence of an interaction between QDs and cellulose. FESEM of cellulose showed porous and homogenous surface morphology, see Figure 2b. The presence of Cd and Te was also investigated using EDX analysis and Figure 3 shows the elemental analysis of the cellulose-CdTeQD composite film. The EDX spectrum showed eight peaks at 2.06, 0.40, 0.55, 1.01, 2.33, 2.61, 3.12, and 3.66 KeV, corresponding to carbon (C), nitrogen (N), oxygen (O), sodium (Na), sulfur (S), chlorine (Cl), cadmium (Cd), and tellurium (Te), respectively. Background peaks at 0.93, 1.74, 2.12, and 3.31 KeV attribute to copper (Cu), silicon (Si), gold (Au), and potassium (K), which come from the initial sample preparation. All these energy values are consistent with the energy values reported previously [44,48]. EDX analysis further confirms that CdTe QDs are anchored on the surface of the cellulose film.

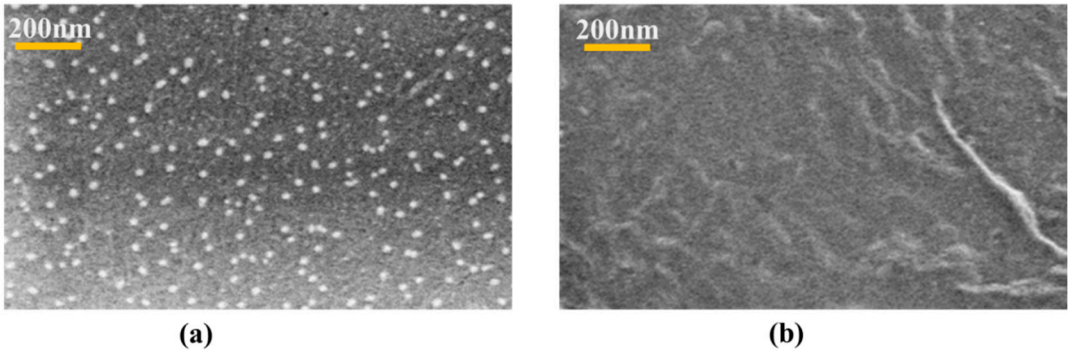

Figure 2. FESEM images of (**a**) cellulose-CdTeQD composite film and (**b**) cellulose film.

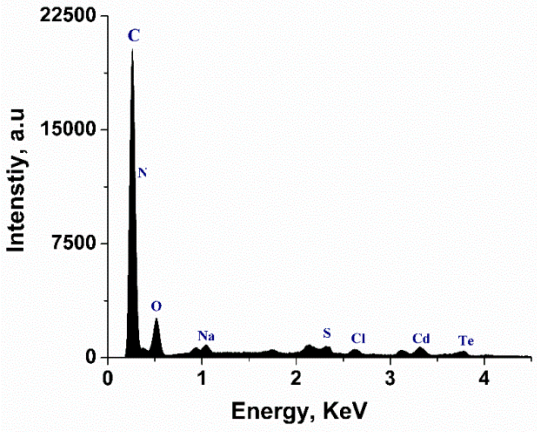

Figure 3. EDX spectrum of cellulose-CdTe QDs film.

3.3. FTIR Chemical Analysis

FTIR analyses were performed on both cellulose-CdTe QDs composite and cellulose films to study and compare the changes in their chemical structure. The FTIR spectra of cellulose-CdTe QDs and cellulose films are shown in Figure 4. The FTIR spectrum of cellulose-CdTe QDs film is similar to that of cellulose film with the exception of an additional peak observed at 1730 cm^{-1}, assigned to cellulose-CdTe QDs film. This peak corresponds to the characteristic antisymmetric C=O vibration of COOH group in GSH [49]. However, it seems that the interaction between COOH group of GSH and O–H groups of cellulose leads to a shift in the antisymmetric C=O band of GSH from 1715 cm^{-1} to 1730 cm^{-1}. The broad peak in the IR region 3700–3100 cm^{-1} is due to O–H stretching vibrations and the extensive inter- and intra-hydrogen bonding. Symmetric and asymmetric stretching vibrations $–CH_2$ of cellulose are observed in the 3000–2800 cm^{-1} region [50,51]. The bands at 1640 and 1439 cm^{-1} are due to O–H bending of physically adsorbed water and O–H in-plane deformation [50]. Bending vibration of C–H is visible at 1372 cm^{-1}. The bands at 1158 and 1104 cm^{-1} are assigned to anti-symmetrical bridge of C–O–C stretching and anti-symmetric in-plane stretching vibrations [50]. The vibrations at 1054 and 1025 cm^{-1} are attributed to C–O stretching vibrations [50]. The peaks at 990 and 894 cm^{-1} are attributed to C–O ring stretching and β-linkage of cellulose [50,52]. The bands at 1315 and 709 cm^{-1} are assigned to $–CH_2$ rocking mode. The absorption peak at 664 cm^{-1} is assigned to O–H out-of-plane bending [50,52]. The similar FTIR spectral pattern for both cellulose film and cellulose-CdTe QDs film suggests that the basic chemical structure of the cellulose is retained during the formation of the composite and there may not be strong interaction between the QDs and cellulose in the composite. Interestingly, our FTIR results of the cellulose-CdTe QDs film are constituent with the chitin-CdTe QDs film reported previously [44].

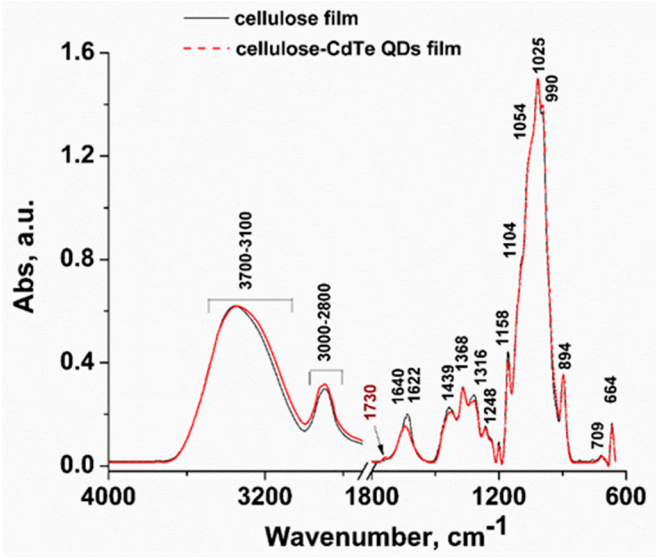

Figure 4. Fourier transform infrared (FTIR) spectra of cellulose and cellulose-CdTe QDs films.

3.4. Thermal Analysis

Thermogravimetric analysis (TGA) was conducted to investigate the thermal stability of the cellulose and cellulose-CdTe QDs films. Figure 5a,b show the thermogravimetric (TG) and derivative thermogravimetric (DTG) profiles of cellulose and cellulose-CdTe QDs composite films. As shown in Figure 5a, the TG profile obtained for cellulose film displays two weight loss regions in the temperature ranges of 35–180 °C and 250–450 °C, corresponding to the evaporation of physically absorbed water and to the thermal degradation of cellulose, respectively. The cellulose-CdTe QDs film show three weight loss regions in 35–180, 250–356, and 356–450 °C temperature ranges, respectively, which are attributed to the evaporation of physically adsorbed water, degradation of cellulose, and decomposition of GSH. The percent weight losses of cellulose and cellulose-CdTe QDs films are 75% and 66%, respectively. The DTG profile of cellulose exhibits a thermal degradation peak at 356 °C, see Figure 5b. However, the DTG profile of cellulose-CdTe QDs film displays two degradation peaks at 342 and 371 °C, reflecting cellulose and GSH, see Figure 5b. Our DTG results suggest that both cellulose and cellulose-CdTe QDs films have similar thermal stability. Furthermore, these results are in agreement with the TGA analysis of chitin-CdTe QDs film reported earlier [44].

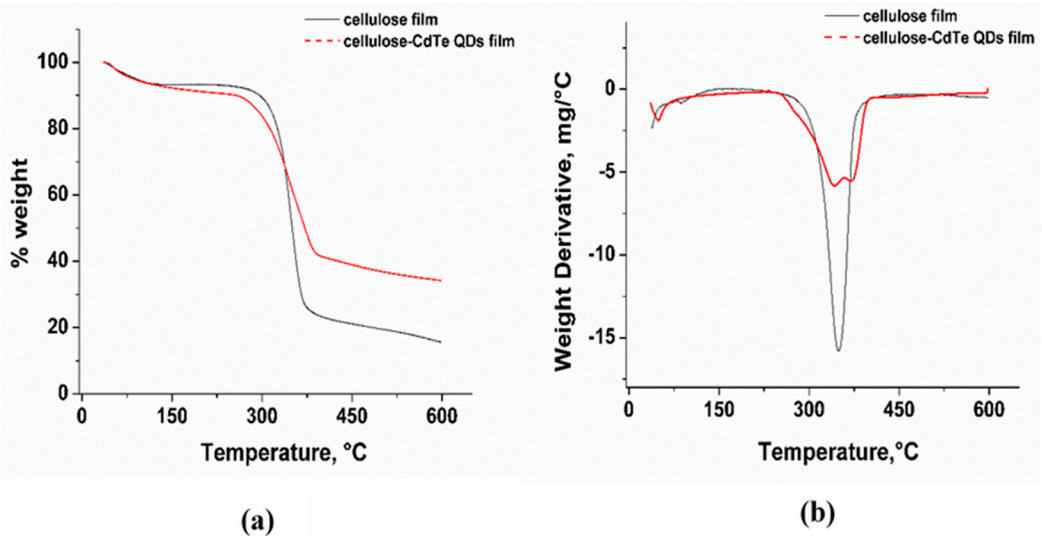

Figure 5. (**a**) TG profiles of cellulose film and cellulose-CdTe QDs film and corresponding (**b**) derivative thermogravimetric (DTG) profiles.

3.5. XRD Analysis

Wide-angle XRD measurements were also conducted for cellulose and cellulose-CdTe QDs films. Both films showed similar diffraction pattern and the diffraction peaks are in agreement with the literature values reported for cellulose (data not shown). However, the peak intensities for cellulose-CdTe QDs are lower, suggesting that the composite is more amorphous in nature as compared to the cellulose film. Moreover, no peaks were observed for CdTe QDs due to the low concentration and low crystallinity of the composite.

3.6. Antibacterial Activity Tests

The antibacterial activity of cellulose and cellulose-CdTe QDs films against the antibiotic resistance bacteria, *S. aureus (+ve)*, was screened. The efficiency of the antimicrobial activity was measured by the agar disk diffusion test after 24 h incubation at 37 °C. Figure 6a,b illustrate the antibacterial effect of cellulose film and cellulose-CdTe QDs film on *S. aureus*. The control sample with only cellulose film did not inhibit the growth of *S. aureus* AH133, see Figure 6a. In contrast, the cellulose-CdTe QDs composite film QDs exhibited a strong inhibitory effect, see Figure 6b. Our results also suggest that the antibacterial activity is mainly due to the embedded CdTe QDs. The average diameter of the growth inhibition zone from cellulose-CdTe QDs film on *S. aureus* was 25 mm, see Figure 6b. This suggests that the growth inhibition factor was released from the CdTe QDs film and reached bacteria that were at a distance from the film. Therefore, the cellulose-CdTe QDs composite film can act as an excellent antibacterial agent against *S. aureus*.

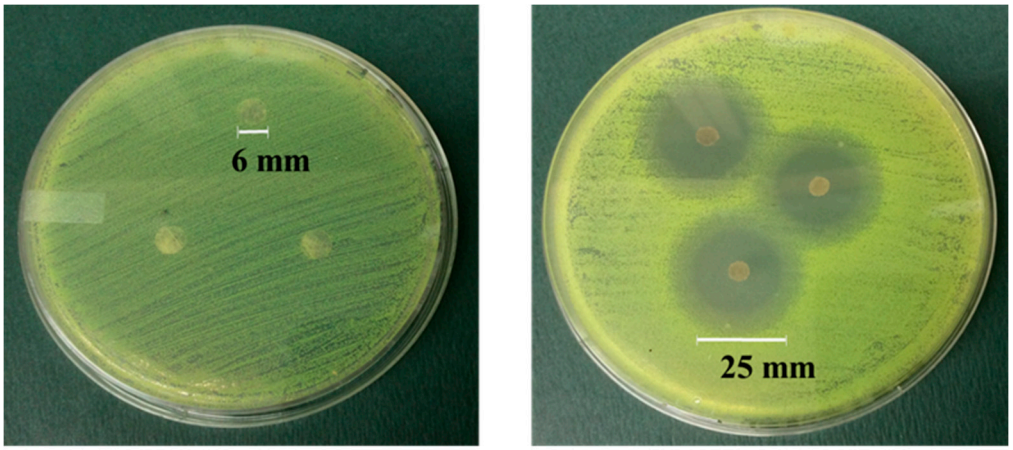

Figure 6. Antibacterial activity of (**a**) cellulose film and (**b**) cellulose-CdTe QDs film on *S. aureus*.

For quantitative assessment of the ability of cellulose-CdTe QDs film to inhibit *S. aureus* AH133 biofilms, we used microtiter plate assay. The growth inhibition was measured by counting the number of colonies formed after keeping the films in a bacterial culture of *S. aureus* for 24 h at 37 °C. As can been seen in Figure 7, an average of over 10^9 CFUs/disk was present on the control cellulose film. In contrast, a significant decrease in the formation of CFUs was observed by the presence of cellulose-CdTe QDs film. The composite film reduced the bioburden by 6 logs. It is worth noting that, this inhibition was achieved with a low concentration of CdTe QDs (1% (*w*/*w*), w.r.t cotton weight). Therefore, a complete inhibition of the biofilm formation may be achieved with a slightly higher concertation of CdTe QDs. These results reveal that cellulose-CdTe QDs film is efficient in eliminating the development of AH133 biofilm.

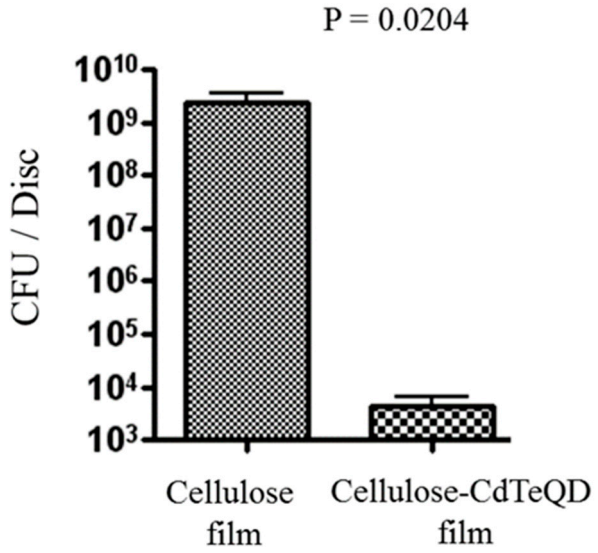

Figure 7. Cellulose-CdTe QDs film significantly reduced biofilm development by *S. aureus* GFP AH133. Cellulose and cellulose-CdTe QDs films were inoculated with *S. aureus* GFP AH133 and incubated for 24 h at 37 °C. The CFU determination is per disk (6 mm diameter and approximately 1 mm thick) in 1 mL solution. Values represent the average of three independent disks ± SEM, $p = 0.0204$.

To further confirm these results, biofilms were allowed to grow on cellulose and cellulose-CdTe QDs for 24 h at 37 °C and were visualized by CLSM, see Figure 8. *S. aureus* contained a gene for GFP which is essential for the visualization of the biofilm. Mature well-developed AH133 biofilm was observed on cellulose film, see Figure 8a. While in the presence of CdTe QDs, only very few scattered microorganisms were detected, see Figure 8b. Thus, cellulose-CdTe QDs film is effective in preventing biofilm formation by *S. aureus*.

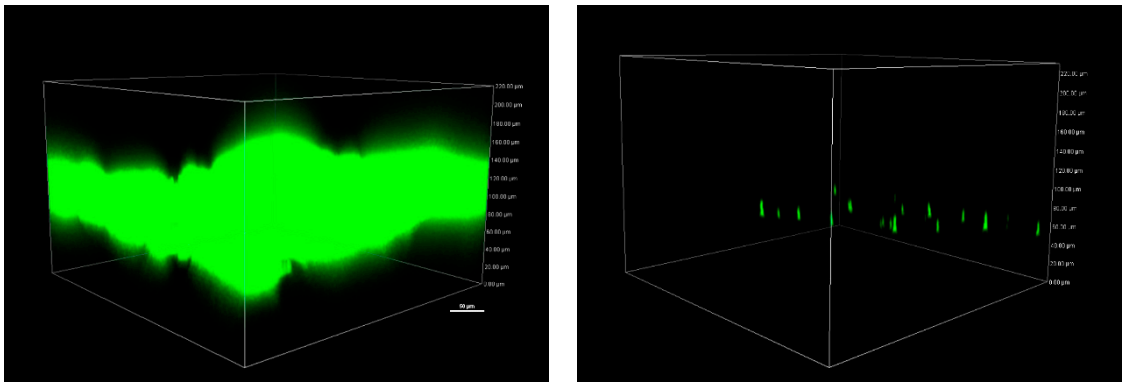

(**a**) (**b**)

Figure 8. 3D-generated confocal laser scanning microscopy (CLSM) images of biofilm formation on (**a**) cellulose and (**b**) cellulose-CdTeQD films in the presence of *S. aureus* GFP AH133.

The antibacterial activity and mechanisms of QDs against both Gram-positive (+*ve*) and Gram-negative (−*ve*) bacterial strains have been studied elsewhere [53–57]. Due to their large particle size, QDs do not penetrate through the cell membrane of the bacteria and consequently kill them. Two main proposed mechanisms suggest (1) a disruption of the membrane functionality by interacting with the cell membranes, and (2) extensive irreversible oxidative damage of cell structures caused by the formation of reactive oxygen species (ROS) including singlet oxygen, superoxide, and hydroxyl radicals. However, the latter ROS-mediated pathway has commonly been reported.

Only a few studies are available for the antibacterial activity of composite materials prepared from chalcogenides-derived QDs against *S. aureus*. For instance, Kumar and coworkers prepared a

chitosan-L-cystein functionalized CdTe QDs film and demonstrated its antibacterial activity against gram-positive (*S. aureus*) and gram-negative (*Pseudomonas aeruginosa* (*P. aeruginosa*) and *Escherichia coli* (*E. coli*)) bacteria by disk diffusion method [56]. Abdelhamid et al. reported the use of chitosan modified CdS QDs composite as a biosensor for both gram-positive (*S. aureus*) and gram-negative (*P. aeruginosa* and *E. coli*) bacteria [57]. Neelgund and coworkers developed two antimicrobial nanohybrids, *f*-MWCNTs-Ag_2S and *f*-MWCNTs-CdS, by functionalizing of multiwalled carbon nanotubes (MWCNTs) with covalent conjugation of cationic hyperbranched dendritic polyamidoamine (PAMAM) and subsequent deposition of Ag_2S and CdS QDs [58]. They also demonstrated the antibacterial activity of those *f*-MWCNTs-QDs nanohybrids against both gram-positive (*S. aureus*) and gram-negative (*P. aeruginosa* and *E. coli*) bacteria [58]. Luo et al. studied the cooperative antibacterial activity of CdTe QDs-rocephin complex against gram-negative *E. coli* bacteria [59]. Park and coworkers also synthesized a polmyxin B-CdTe QDs (CdTe-PMB) conjugate and studied its ability to act against both gram-positive (*S. aureus*) and gram-negative (*E. coli*) bacteria [60]. They reported that CdTe-PMB is more effective against *E. coli* as compared to *S. aureus* [60]. We previously investigated the antibacterial activity of chitin-CdTe QDs hybrid material against gram-positive (*S. aureus*) and gram-negative (*P. aeruginosa*) bacteria [44]. Chitin-CdTe QDs hybrid material showed antibacterial activity against both *S. aureus* and *P. aeruginosa* bacteria. During the various stages in the process of converting cotton fibers into yarn and then yarn into fabric, about 1/3 of cotton is discarded as waste due to fiber immaturity, short fiber length, lower fineness, and poor quality. Generally, waste cotton is either landfilled or incinerated [61,62]. These disposing methods now have become a serious environmental concern mainly due to the contamination of soil and natural water sources [63]. Therefore, many attempts are currently underway to recycle or convert these waste cotton materials into value-added products for both environmental and economic aspects [63–67]. In this study, we successfully fabricated CdTe QDs on the cellulose films prepared from waste cotton linters. Importantly, our control experiments did not show any leaching of QDs, suggesting the stability of QDs in the polymer matrix. The cellulose-CdTe QDs composite film displayed a significant inhibition of biofilm-formation by *S. aureus*, which is considered as one of the most multidrug-resistant bacteria. Therefore, this study paves the way to reduce the environmental burden and also add value to waste cotton. This process can also be translated into commercial biomedical applications due to the low processing cost, environmental benignity, natural abundance, and scalability.

4. Conclusions

In summary, cellulose-CdTe QDs composite films were successfully synthesized using a simple process. CdTe QDs were homogenously fabricated on the cellulose film prepared from waste cotton linters. Cellulose-CdTe QDs (1% (*w*/*w*) w.r.t cellulose) composite film exhibited a good inhibition against antibiotic resistance against biofilm forming *S. aureus* (gram-positive) bacteria. The porous 3D network of cellulose film acted as a stable dispersion support and also prevented QDs from self-aggregation. Therefore, this material could be desirable in many biomedical applications including wound dressing, antimicrobial packing, burn treatments, and medical devices, and in implants.

Author Contributions: These authors contributed equally.

Funding: This research received no external funding.

Acknowledgments: The authors would like to thank Texas Tech University Graduate School and the Fiber and Biopolymer Research Institute for providing final support.

Conflicts of Interest: The authors declare no conflict of interest.

References

1. Kobayashi, S.D.; Malachowa, N.; DeLeo, F.R. Pathogenesis of Staphylococcus aureus Abscesses. *Am. J. Pathol.* **2015**, *185*, 1518–1527. [CrossRef] [PubMed]

2. Tong, S.Y.C.; Davis, J.S.; Eichenberger, E.; Holland, T.L.; Fowler, V.G. Staphylococcus aureus Infections: Epidemiology, Pathophysiology, Clinical Manifestations, and Management. *Clin. Microbiol. Rev.* **2015**, *28*, 603–661. [CrossRef] [PubMed]
3. Gould, D.; Chamberlaine, A. Staphylococcus ureus: A review of the literature. *J. Clin. Nurs.* **1995**, *4*, 5–12. [CrossRef] [PubMed]
4. Thomer, L.; Schneewind, O.; Missiakas, D. Pathogenesis of Staphylococcus aureus Bloodstream Infections. *Annu. Rev. Pathol. Mech. Dis.* **2016**, *11*, 343–364. [CrossRef] [PubMed]
5. Pantosti, A.; Sanchini, A.; Monaco, M. Mechanisms of antibiotic resistance in Staphylococcus aureus. *Future Microbiol.* **2007**, *2*, 323–334. [CrossRef] [PubMed]
6. Chambers, H.F.; DeLeo, F.R. Waves of Resistance: Staphylococcus aureus in the Antibiotic Era. *Nat. Rev. Microbiol.* **2009**, *7*, 629–641. [CrossRef] [PubMed]
7. Yoshii, Y.; Okuda, K.-I.; Yamada, S.; Nagakura, M.; Sugimoto, S.; Nagano, T.; Okabe, T.; Kojima, H.; Iwamoto, T.; Kuwano, K.; et al. Norgestimate inhibits staphylococcal biofilm formation and resensitizes methicillin-resistant Staphylococcus aureus to β-lactam antibiotics. *NPJ Biofilms Microbiomes* **2017**, *3*, 18. [CrossRef] [PubMed]
8. Melchior, M.B.; Vaarkamp, H.; Fink-Gremmels, J. Biofilms: A role in recurrent mastitis infections? *Vet. J. (Lond. Engl. 1997)* **2006**, *171*, 398–407. [CrossRef]
9. Song, M.; Li, Q.; Zhang, Y.; Song, J.; Shi, X.; Shi, C. Biofilm formation and antibiotic resistance pattern of dominant Staphylococcus aureus clonal lineages in China. *J. Food Saf.* **2017**, *37*, e12304. [CrossRef]
10. Costerton, J.W.; Stewart, P.S.; Greenberg, E.P. Bacterial biofilms: A common cause of persistent infections. *Sci. (N. Y.)* **1999**, *284*, 1318–1322. [CrossRef]
11. Khan, A.U.; Sultan, A.; Tyagi, A.; Zahoor, S.; Akram, M.; Kaur, S.; Shahid, M.; Vaishnavi, C.V. Amplification of mecA gene in multi-drug resistant Staphylococcus aureus strains from hospital personnel. *J. Infect. Dev. Ctries.* **2007**, *1*, 289–295. [CrossRef] [PubMed]
12. Suhas Gupta, V.K.; Carrott, P.J.M.; Singh, R.; Chaudhary, M.; Kushwaha, S. Cellulose: A review as natural, modified and activated carbon adsorbent. *Bioresour. Technol.* **2016**, *216*, 1066–1076. [CrossRef] [PubMed]
13. Ummartyotin, S.; Manuspiya, H. A critical review on cellulose: From fundamental to an approach on sensor technology. *Renew. Sustain. Energy Rev.* **2015**, *41*, 402–412. [CrossRef]
14. Wang, X.; Yao, C.; Wang, F.; Li, Z. Cellulose-Based Nanomaterials for Energy Applications. *Small (Weinh. Bergstr. Ger.)* **2017**, *13*. [CrossRef] [PubMed]
15. Czaja, W.K.; Young, D.J.; Kawecki, M.; Brown, R.M. The Future Prospects of Microbial Cellulose in Biomedical Applications. *Biomacromolecules* **2007**, *8*, 1–12. [CrossRef] [PubMed]
16. Rezaei, A.; Nasirpour, A.; Fathi, M. Application of Cellulosic Nanofibers in Food Science Using Electrospinning and Its Potential Risk. *Compr. Rev. Food Sci. Food Saf.* **2015**, *14*, 269–284. [CrossRef]
17. Li, S.; Huang, J.; Chen, Z.; Chen, G.; Lai, Y. A review on special wettability textiles: Theoretical models, fabrication technologies and multifunctional applications. *J. Mater. Chem. A* **2017**, *5*, 31–55. [CrossRef]
18. Sulaeva, I.; Henniges, U.; Rosenau, T.; Potthast, A. Bacterial cellulose as a material for wound treatment: Properties and modifications. A review. *Biotechnol. Adv.* **2015**, *33*, 1547–1571. [CrossRef] [PubMed]
19. Wang, J.; Vermerris, W. Antimicrobial Nanomaterials Derived from Natural Products—A Review. *Materials* **2016**, *9*, 255. [CrossRef] [PubMed]
20. Naseri-Nosar, M.; Ziora, Z.M. Wound dressings from naturally-occurring polymers: A review on homopolysaccharide-based composites. *Carbohydr. Polym.* **2018**, *189*, 379–398. [CrossRef] [PubMed]
21. Portela, R.; Leal, C.R.; Almeida, P.L.; Sobral, R.G. Bacterial cellulose: A versatile biopolymer for wound dressing applicaions. *Microb. Biotechnol.* **2019**, *12*, 586–610. [CrossRef] [PubMed]
22. Fernandes, S.C.M.; Sadocco, P.; Alonso-Varona, A.; Palomares, T.; Eceiza, A.; Silvestre, A.J.D.; Mondragon, I.; Freire, C.S.R. Bioinspired Antimicrobial and Biocompatible Bacterial Cellulose Membranes Obtained by Surface Functionalization with Aminoalkyl Groups. *ACS Appl. Mater. Interfaces* **2013**, *5*, 3290–3297. [CrossRef]
23. Saini, S.; Belgacem, M.N.; Salon, M.-C.B.; Bras, J. Non leaching biomimetic antimicrobial surfaces via surface functionalisation of cellulose nanofibers with aminosilane. *Cellulose* **2016**, *23*, 795–810. [CrossRef]
24. Roemhild, K.; Wiegand, C.; Hipler, U.C.; Heinze, T. Novel bioactive amino-functionalized cellulose nanofibers. *Macromol. Rapid Commun.* **2013**, *34*, 1767–1771. [CrossRef] [PubMed]

25. Jian, W.; Yudong, Z.; Xiaoxiao, W.; Qinghua, L.; Xiaohua, C.; Zhigu, W. Silver nanoparticle/bacterial cellulose gel membranes for antibacterial wound dressing: Investigation in vitro and in vivo. *Biomed. Mater.* **2014**, *9*, 035005.
26. Barud, H.S.; Regiani, T.; Marques, R.F.C.; Lustri, W.R.; Messaddeq, Y.; Ribeiro, S.J.L. Antimicrobial Bacterial Cellulose-Silver Nanoparticles Composite Membranes. *J. Nanomater.* **2011**, *2011*, 8. [CrossRef]
27. Jia, B.; Mei, Y.; Cheng, L.; Zhou, J.; Zhang, L. Preparation of copper nanoparticles coated cellulose films with antibacterial properties through one-step reduction. *ACS Appl. Mater. Interfaces* **2012**, *4*, 2897–2902. [CrossRef] [PubMed]
28. Eivazihollagh, A.; Bäckström, J.; Dahlström, C.; Dahlström, C.; Carlsson, F.; Ibrahem, I.; Lindman, B.; Edlund, H.; Norgren, M. One-pot synthesis of cellulose-templated copper nanoparticles with antibacterial properties. *Mater. Lett.* **2017**, *187*, 170–172. [CrossRef]
29. Luo, Y.; Huang, J. Hierarchical-Structured Anatase-Titania/Cellulose Composite Sheet with High Photocatalytic Performance and Antibacterial Activity. *Chem. Eur. J.* **2015**, *21*, 2568–2575. [CrossRef] [PubMed]
30. Khalid, A.; Ullah, H.; Ul-Islam, M.; Khan, R.; Khan, S.; Ahmad, F.; Khan, T.; Wahid, F. Bacterial cellulose-TiO2 nanocomposites promote healing and tissue regeneration in burn mice model. *RSC Adv.* **2017**, *7*, 47662–47668. [CrossRef]
31. Fu, F.; Li, L.; Liu, L.; Cai, J.; Zhang, Y.; Zhou, J.; Zhang, L. Construction of Cellulose Based ZnO Nanocomposite Films with Antibacterial Properties through One-Step Coagulation. *ACS Appl. Mater. Interfaces* **2015**, *7*, 2597–2606. [CrossRef] [PubMed]
32. Azizi, S.; Ahmad, M.B.; Hussein, M.Z.; Ibrahim, N.A. Synthesis, antibacterial and thermal studies of cellulose nanocrystal stabilized ZnO-Ag heterostructure nanoparticles. *Molecules* **2013**, *18*, 6269–6280. [CrossRef] [PubMed]
33. Courtney, C.M.; Goodman, S.M.; McDaniel, J.A.; Madinger, N.E.; Chatterjee, A.; Nagpal, P. Photoexcited quantum dots for killing multidrug-resistant bacteria. *Nat. Mater.* **2016**, *15*, 529. [CrossRef] [PubMed]
34. Galdiero, E.; Siciliano, A.; Maselli, V.; Gesuele, R.; Guida, M.; Fulgione, D.; Galdiero, S.; Lombardi, L.; Falanga, A. An integrated study on antimicrobial activity and ecotoxicity of quantum dots and quantum dots coated with the antimicrobial peptide indolicidin. *Int. J. Nanomed.* **2016**, *11*, 4199–4211. [CrossRef] [PubMed]
35. He, X.; Ma, N. An overview of recent advances in quantum dots for biomedical applications. *Colloids Surf. B Biointerfaces* **2014**, *124*, 118–131. [CrossRef] [PubMed]
36. Yang, Z.; Fan, J.Z.; Proppe, A.H.; de Arquer, F.P.G.; Rossouw, D.; Voznyy, O.; Lan, X.; Liu, M.; Walters, G.; Quintero-Bermudez, R.; et al. Mixed-quantum-dot solar cells. *Nat. Commun.* **2017**, *8*, 1325. [CrossRef] [PubMed]
37. Kamat, P.V. Quantum Dot Solar Cells. The Next Big Thing in Photovoltaics. *J. Phys. Chem. Lett.* **2013**, *4*, 908–918. [CrossRef] [PubMed]
38. Paivasaari, K.; Tikhomirov, V.K.; Turunen, J. High refractive index chalcogenide glass for photonic crystal applications. *Opt. Express* **2007**, *15*, 2336–2340. [CrossRef] [PubMed]
39. Rizvi, S.B.; Ghaderi, S.; Keshtgar, M.; Seifalian, A.M. Semiconductor quantum dots as fluorescent probes for in vitro and in vivo bio-molecular and cellular imaging. *Nano Rev.* **2010**, *1*. [CrossRef]
40. Cabral Filho, P.E.; Cardoso, A.L.C.; Pereira, M.I.A.; Ramos, A.P.M.; Hallwass, F.; Castro, M.M.C.A.; Geraldes, C.F.G.C.; Santos, B.S.; Pedroso de Lima, M.C.; Pereira, G.A.L.; et al. CdTe quantum dots as fluorescent probes to study transferrin receptors in glioblastoma cells. *Biochim. Et Biophys. Acta (BBA) Gen. Subj.* **2016**, *1860*, 28–35. [CrossRef]
41. Tan, X.; Liu, S.; Shen, Y.; He, Y.; Liu, Y.; Yang, J. Glutathione-capped CdTe quantum dots for the determination of fleroxacin with dual-wavelength fluorescence signals. *Anal. Methods* **2014**, *6*, 4860–4866. [CrossRef]
42. Jacob, J.M.; Lens, P.N.L.; Balakrishnan, R.M. Microbial synthesis of chalcogenide semiconductor nanoparticles: A review. *Microb. Biotechnol.* **2016**, *9*, 11–21. [CrossRef]
43. Yu, W.W.; Chang, E.; Drezek, R.; Colvin, V.L. Water-soluble quantum dots for biomedical applications. *Biochem. Biophys. Res. Commun.* **2006**, *348*, 781–786. [CrossRef] [PubMed]
44. Wansapura Poorna, T.; Dassanayake Rohan, S.; Hamood, A.; Tran, P.; Moussa, H.; Abidi, N. Preparation of chitin-CdTe quantum dots films and antibacterial effect on Staphylococcus aureus and Pseudomonas aeruginosa. *J. Appl. Polym. Sci.* **2017**, 134. [CrossRef]

45. Pérez-Donoso, J.M.; Monrás, J.P.; Bravo, D.; Aguirre, A.; Quest, A.F.; Osorio-Román, I.O.; Aroca, R.F.; Chasteen, T.G.; Vásquez, C.C. Biomimetic, Mild Chemical Synthesis of CdTe-GSH Quantum Dots with Improved Biocompatibility. *PLoS ONE* **2012**, *7*, e30741. [CrossRef] [PubMed]
46. Wansapura, P.T.; Diaz-Vasquez, W.A.; Vasquez, C.C.; Perez-Donoso, J.M.; Chasteen, T.G. Thermal and photo stability of glutathione-capped cadmium telluride quantum dots. *J. Appl. Biomater. Funct. Mater.* **2015**, *13*, e248–e252. [CrossRef]
47. Tran, P.L.; Lowry, N.; Campbell, T.; Reid, T.W.; Webster, D.R.; Tobin, E.; Aslani, A.; Mosley, T.; Dertien, J.; Colmer-Hamood, J.A.; et al. An Organoselenium Compound Inhibits Staphylococcus aureus Biofilms on Hemodialysis Catheters In Vivo. *Antimicrob. Agents Chemother.* **2012**, *56*, 972–978. [CrossRef] [PubMed]
48. Haydous, F.; Halaoui, L. Quantum-Confined CdTe Films Deposited by SILAR and Their Photoelectrochemical Stability in the Presence of Se2– as a Hole Scavenger. *J. Phys. Chem. C* **2014**, *118*, 18334–18342. [CrossRef]
49. Monrás, J.P.; Díaz, V.; Bravo, D.; Montes, R.A.; Chasteen, T.G.; Osorio-Román, I.O.; Vásquez, C.C.; Pérez-Donoso, J.M. Enhanced Glutathione Content Allows the In Vivo Synthesis of Fluorescent CdTe Nanoparticles by Escherichia coli. *PLoS ONE* **2012**, *7*, e48657. [CrossRef]
50. Abidi, N.; Cabrales, L.; Haigler, C.H. Changes in the cell wall and cellulose content of developing cotton fibers investigated by FTIR spectroscopy. *Carbohydr. Polym.* **2014**, *100*, 9–16. [CrossRef]
51. Dassanayake, R.S.; Gunathilake, C.; Jackson, T.; Jaroniec, M.; Abidi, N. Preparation and adsorption properties of aerocellulose-derived activated carbon monoliths. *Cellulose* **2016**, *23*, 1363–1374. [CrossRef]
52. Abidi, N.; Hequet, E.; Cabrales, L.; Gannaway, J.; Wilkins, T.; Wells, L.W. Evaluating cell wall structure and composition of developing cotton fibers using Fourier transform infrared spectroscopy and thermogravimetric analysis. *J. Appl. Polym. Sci.* **2008**, *107*, 476–486. [CrossRef]
53. Lu, Z.; Li, C.M.; Bao, H.; Qiao, Y.; Toh, Y.; Yang, X. Mechanism of Antimicrobial Activity of CdTe Quantum Dots. *Langmuir* **2008**, *24*, 5445–5452. [CrossRef] [PubMed]
54. Dumas, E.; Gao, C.; Suffern, D.; Bradforth, S.E.; Dimitrijevic, N.M.; Nadeau, J.L. Interfacial Charge Transfer between CdTe Quantum Dots and Gram Negative Vs. Gram Positive Bacteria. *Environ. Sci. Technol.* **2010**, *44*, 1464–1470. [CrossRef] [PubMed]
55. Rameshkumar, A.; Sivasudha, T.; Jeyadevi, R.; Sangeetha, B.; Ananth, D.A.; Aseervatham, G.S.; Nagarajan, N.; Renganathan, R.; Kathiravan, A. In vitro antioxidant and antimicrobial activities of Merremia emarginata using thio glycolic acid-capped cadmium telluride quantum dots. *Colloids Surf. Bbiointerfaces* **2013**, *101*, 74–82. [CrossRef]
56. Kumar, H.; Srivastava, R.; Dutta, P.K. Highly luminescent chitosan-L-cysteine functionalized CdTe quantum dots film: Synthesis and characterization. *Carbohydr. Polym.* **2013**, *97*, 327–334. [CrossRef]
57. Abdelhamid, H.N.; Wu, H.-F. Probing the interactions of chitosan capped CdS quantum dots with pathogenic bacteria and their biosensing application. *J. Mater. Chem. B* **2013**, *1*, 6094–6106. [CrossRef]
58. Neelgund, G.M.; Oki, A.; Luo, Z. Antimicrobial activity of CdS and Ag(2)S quantum dots immobilized on poly(amidoamine) grafted carbon nanotubes. *Colloids Surf. Bbiointerfaces* **2012**, *100*, 215–221. [CrossRef]
59. Luo, Z.; Wu, Q.; Zhang, M.; Li, P.; Ding, Y. Cooperative antimicrobial activity of CdTe quantum dots with rocephin and fluorescence monitoring for Escherichia coli. *J. Colloid Interface Sci.* **2011**, *362*, 100–106. [CrossRef]
60. Soonhyang, P.; Hicham, C.; Jody, W.; Jay, L.N. Antimicrobial activity and cellular toxicity of nanoparticle–polymyxin B conjugates. *Nanotechnology* **2011**, *22*, 185101.
61. Han, Y.; Zhang, X.; Wu, X.; Lu, C. Flame Retardant, Heat Insulating Cellulose Aerogels from Waste Cotton Fabrics by in Situ Formation of Magnesium Hydroxide Nanoparticles in Cellulose Gel Nanostructures. *ACS Sustain. Chem. Eng.* **2015**, *3*, 1853–1859. [CrossRef]
62. He, X.; Zhang, X.; Zhang, W.; Tian, D.; Lu, C. Mechanochemically activated waste-derived cellulose as a novel functional additive to enhance melt processability and mechanical properties of poly (vinyl alcohol). *J. Vinyl Addit. Technol.* **2014**, *20*, 177–184. [CrossRef]
63. Xiong, R.; Zhang, X.; Tian, D.; Zhou, Z.; Lu, C. Comparing microcrystalline with spherical nanocrystalline cellulose from waste cotton fabrics. *Cellulose* **2012**, *19*, 1189–1198. [CrossRef]
64. Huang, F.; Xu, Y.; Peng, B.; Su, Y.; Jiang, F.; Hsieh, Y.-L.; Wei, Q. Coaxial Electrospun Cellulose-Core Fluoropolymer-Shell Fibrous Membrane from Recycled Cigarette Filter as Separator for High Performance Lithium-Ion Battery. *ACS Sustain. Chem. Eng.* **2015**, *3*, 932–940. [CrossRef]

65. Lam, E.; Leung, A.C.W.; Liu, Y.; Majid, E.; Hrapovic, S.; Male, K.B.; Luong, J.H.T. Green Strategy Guided by Raman Spectroscopy for the Synthesis of Ammonium Carboxylated Nanocrystalline Cellulose and the Recovery of Byproducts. *ACS Sustain. Chem. Eng.* **2013**, *1*, 278–283. [CrossRef]
66. Salam, A.; Lucia, L.A.; Jameel, H. A Novel Cellulose Nanocrystals-Based Approach to Improve the Mechanical Properties of Recycled Paper. *ACS Sustain. Chem. Eng.* **2013**, *1*, 1584–1592. [CrossRef]
67. Xiao, L.; Mai, Y.; He, F.; Yu, L.; Zhang, L.; Tang, H.; Yang, G. Bio-based green composites with high performance from poly (lactic acid) and surface-modified microcrystalline cellulose. *J. Mater. Chem.* **2012**, *22*, 15732–15739. [CrossRef]